Bioactive Materials 5 (2020) 1062–1070

Contents lists available at ScienceDirect

Bioactive Materials

journal homepage: http://www.keaipublishing.com/biomat

Effect of size and crystalline phase of TiO_2 nanotubes on cell behaviors: A high throughput study using gradient TiO_2 nanotubes

Yanran Li[a], Si Wang[a], Yuanjun Dong[a], Ping Mu[a], Yun Yang[a], Xiangyang Liu[a,b], Changjian Lin[c], Qiaoling Huang[a,*]

[a] Research Institute for Biomimetics and Soft Matter, Fujian Provincial Key Laboratory for Soft Functional Materials Research, Department of Physics, College of Physical Science and Technology, Xiamen University, Xiamen, 361005, China
[b] Department of Physics, National University of Singapore, 2 Science Drive 3, 117542, Singapore
[c] State Key Laboratory for Physical Chemistry of Solid Surfaces, Department of Chemistry, College of Chemistry and Chemical Engineering, Xiamen University, Xiamen, 361005, China

ARTICLE INFO

Keywords:
Gradient TiO_2 nanotubes
High-throughput screening
Protein adsorption
Cell proliferation
Cell differentiation

ABSTRACT

The research of TiO_2 nanotubes (TNTs) in the field of biomedicine has been increasingly active. However, given the diversity of the nanoscale dimension and controversial reports, our understanding of the structure-property relationships of TNTs is not yet complete. In this paper, gradient TNTs with a wide diameter range of 20–350 nm were achieved by bipolar electrochemistry and utilized for a thorough high-throughput study of the effect of nanotube dimension and crystalline phase on protein adsorption and cell behaviors. Results indicated that protein adsorption escalated with nanotube dimension whereas cell proliferation and differentiation are preferred on small diameter (< 70 nm) nanotubes. Large diameter anatase nanotubes had higher adsorption of serum proteins than as-prepared ones. But only as-prepared small diameter nanotubes presented slightly higher cell proliferation than corresponding annealed nanotubes whereas there was no discernible difference between as-prepared and annealed nanotubes on cell differentiation for the entire gradient. Those findings replenish previous research about how cell responses to TNTs with a wide diameter range and provide scientific guidance for the optimal design of biomedical materials.

1. Introduction

Titanium-based biomedical materials have been widely used for load-bearing applications because of their terrific biocompatibility, corrosion resistance, and mechanical properties [1,2]. However, failure in clinical applications is often inevitable because the implant surface with inadequate bioactivity is prone to form fibrous tissue in the body, resulting in its insufficient bone-bonding ability. Hence, it is imperative to improve the bioactivity of titanium-based materials [3–5].

Over the past decade, self-aligned TiO_2 nanotubes (TNTs) grown on titanium have been extensively developed in environmental protection, photocatalysis [6–8], sensors [9,10], dye-sensitized solar cells [11,12], and biomedical applications [13–15] owing to their superior high-specific surface area, specific ion intercalation properties, photocatalysis property, and cost-effective synthesis. In particular, the terrific biocompatibility, corrosion resistance and size controllable properties of TNTs make them promising for biomedical applications, such as orthopedic/dental implants [16,17], blood contact materials [18], antimicrobial application [19,20], and drug delivery [21,22].

It is well known that biomaterials surface properties (such as chemistry, morphology, roughness, wettability) play an essential role in the association between implants and biomaterials. It is found that both morphology diversity and crystalline phases could affect cell responses to TNTs [13,23,24]. However, there is no consistency in the literature. Some research groups demonstrated that TNTs with the smallest nanotube diameter promoted the highest cell proliferation and/or differentiation [25–28] whereas some groups proved controversial results, or even opposite [29–31]. Some studies indicated that annealed nanotubes could facilitate cell proliferation [32,33] whereas some studies found different results [34,35]. Moreover, the nanotube diameter could range from a few nm to hundreds of nm, which not only provides infinite possibilities but also poses great challenges. Most researches randomly chose a few dimensions (mostly within 120 nm) for a study that it remains obscure how cells respond to large nanotubes. But it is impossible

Peer review under responsibility of KeAi Communications Co., Ltd.
* Corresponding author.
E-mail address: qlhuang@xmu.edu.cn (Q. Huang).

https://doi.org/10.1016/j.bioactmat.2020.07.005
Received 1 April 2020; Received in revised form 8 July 2020; Accepted 10 July 2020

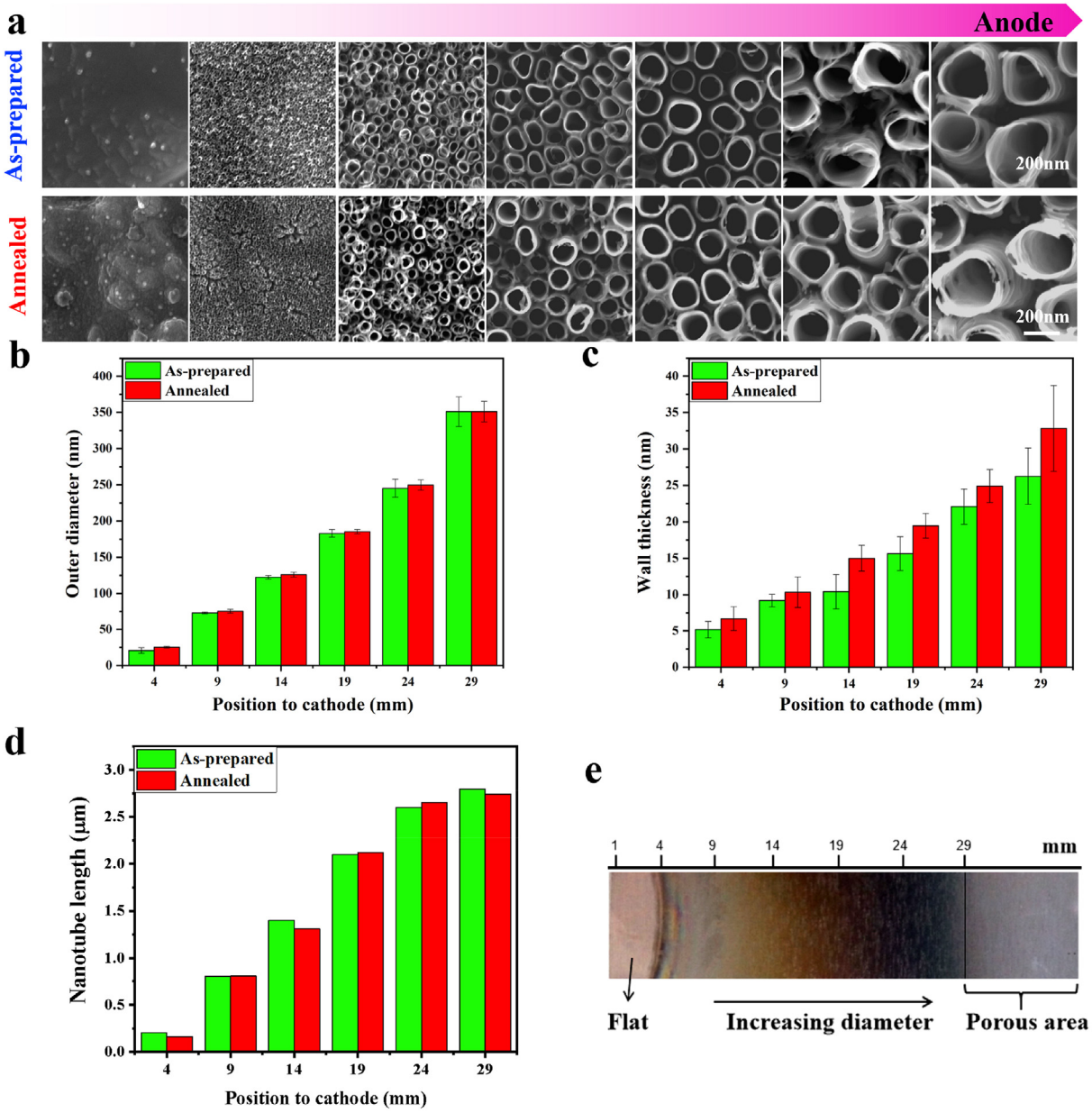

Fig. 1. (a) FE-SEM views of the as-prepared and annealed gradient TiO_2 nanotube arrays starting from the cathode edge to the anode edge. The outer diameter (b), wall thickness (c), and nanotube length (d) of TiO_2 nanotubes vary with the position of BPE. (e) The macroscopic optical image of as-prepared gradient TNTs.

to thoroughly investigate cell responses to all dimensions using a conventional method.

Since the protein micropattern was realized by MacAlear and Wehrung in 1978 [36], micropatterning techniques manifest extraordinary advantages in high-throughput screening of biomaterials surface properties [37,38]. Several attempts have been made to fabricate micropatterned nanotubes to solve the above problems. Andreas achieved micropatterned TiO_2 nanotube arrays (with a diameter of 15 nm and 100 nm) and directly compared stem cell behavior on different diameter nanotubes [39]. Yifan fabricated and utilized TiO_2 nanotube arrays with four coexisting diameters (60, 150, 250, and 350 nm) to investigate cell behaviors [40]. We previously constructed gradient TNTs (diameter range 30–100 nm) and demonstrated that cell proliferation and differentiation diminished with the nanotube dimension [28]. However, it remains obscure if this rule is applicable to a wider range of nanotubes.

In this study, we applied bipolar electrochemistry to fabricate gradient TiO_2 nanotube arrays (GTNTs) with a wider diameter range (from 20 to 350 nm). GTNTs were further annealed to obtain crystalline phases. Both as-prepared and annealed GTNTs were utilized for investigation of size and crystalline phase effects on protein adsorption and cellular responses.

2. Materials and methods

2.1. Preparation of gradient TiO_2 nanotube arrays

Titanium foils (0.1 mm think, 99.6% purity) of 38 × 10 mm were first degreased by sonication in acetone, ethanol, and deionized water for 20 min. Then foils were etched in a water solution consisting of 1% HF and 10% HNO_3 for 2 min, followed by water rinsing and air drying. The electrolyte utilized for fast-growing large gradient TiO_2 nanotube arrays was composed of 0.75 wt% NH_4F, 10 vol% H_2O and 90 vol% glycerol. Ti foil served as a working electrode and was tapped on the bottom of a weighing dish. A pair of platinum plates served as feeder electrodes fixing on a weighing dish at 1 mm from Ti foil. The reaction

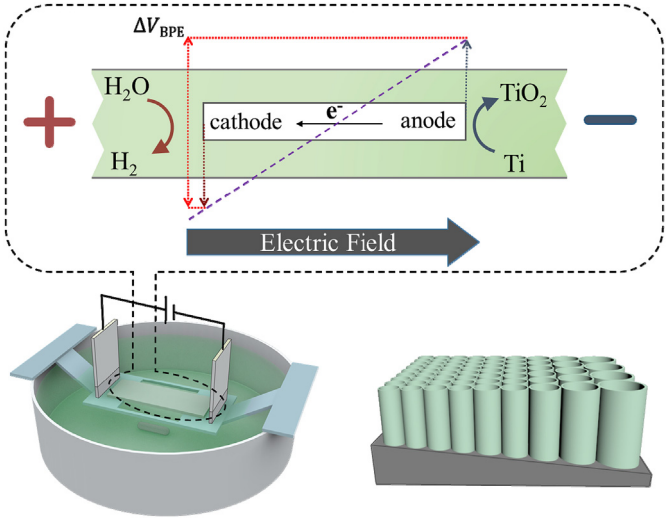

Scheme 1. Illustration of bipolar electrochemistry.

was conducted at 15 °C under a voltage of 180 V for 3 h, followed by water washing and air drying. The annealed samples were achieved by annealing the as-prepared samples at 450 °C for 2 h. Samples were irradiated with ultraviolet light for sterilization. Samples were examined thoroughly across the entire gradient for all following experiments. But only seven positions (including the flat area) on the sample were selected for representation, i.e., starting from the smallest nanotube, images were taken every 5 mm till the largest nanotubes (Fig. 1e).

2.2. Characterization

The surface morphology of the gradient samples was inspected by scanning electron microscopy (FE-SEM, Oxford Zeiss Sigma). Some scratches (Fig. S1a, indicated by the red arrow) were created by a tweezer on the surface and used as marks to locate the TNTs under FE-SEM. The crystalline phases at different positions of samples were qualitatively analyzed by X-ray diffractometer (XRD, Bruker-axs) and Confocal Raman spectrometer (WITec alpha 300RA). Different positions of the gradient TNTs were aligned with the X-ray beam or Raman laser to investigate crystalline phase changes across the gradients.

2.3. Protein labeling and adsorption

Protein adsorption was investigated by detecting the fluorescence intensity of adsorbed protein labeled with fluorescein isothiocyanate (FITC, Sigma). Bovine serum albumin (BSA, Sigma) and fetal bovine serum (FBS, Gibco) were diluted in phosphate-buffered saline (PBS) to 5 mg/ml and 10 vol%, respectively. FITC was diluted in DMSO to 5 mg/ml and mixed with protein solution at the ratio of 1:100. Then sodium carbonate was added to the concentration of 500 mM and stirred for 2 h in the dark before dialyzing at 4 °C for 3 days to remove excess unbound FITC. Labeled proteins were stored in a refrigerator at 4 °C and used within two weeks. The labeled protein solution was cultured on the sample surface for 30 min in a 37 °C incubator. Then samples were washed with deionized water and air-dried before imaging. Fluorescent images were photographed by a fluorescence microscope (TCS SP8, Leica, Germany) and analyzed by Image J.

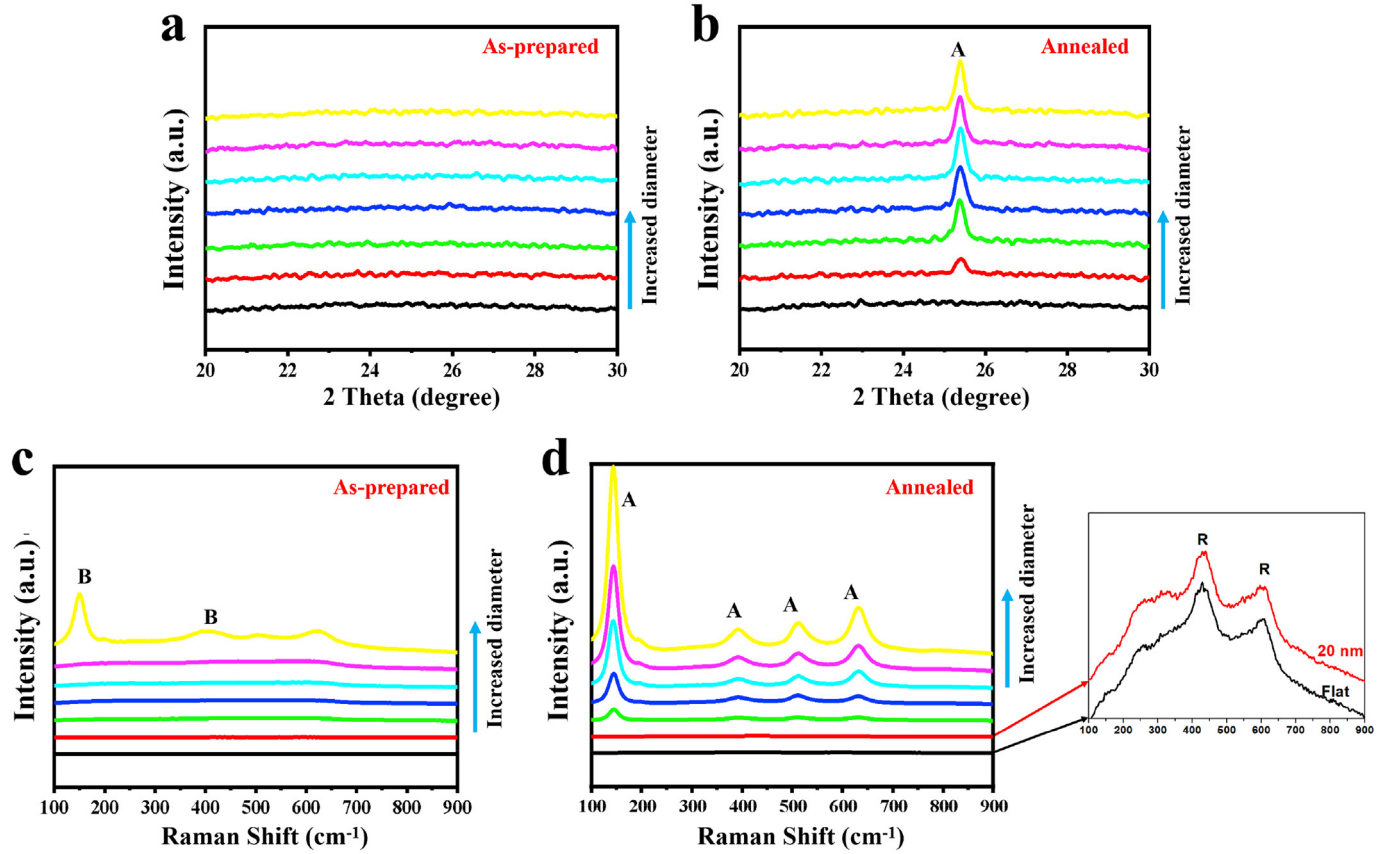

Fig. 2. The XRD patterns (a, b) and Raman spectra (c, d) of the TNTs from different positions of the as-prepared (a, c) and annealed G-TNTs (b, d). Seven spectra in each figure correspond to seven positions on the gradient TNTs as shown in Fig. 1e. "A" presents anatase, "B" presents brookite and "R" presents rutile. The inset image is an enlargement of the Raman spectra of the annealed 20-nm nanotube and flat TiO_2 surfaces.

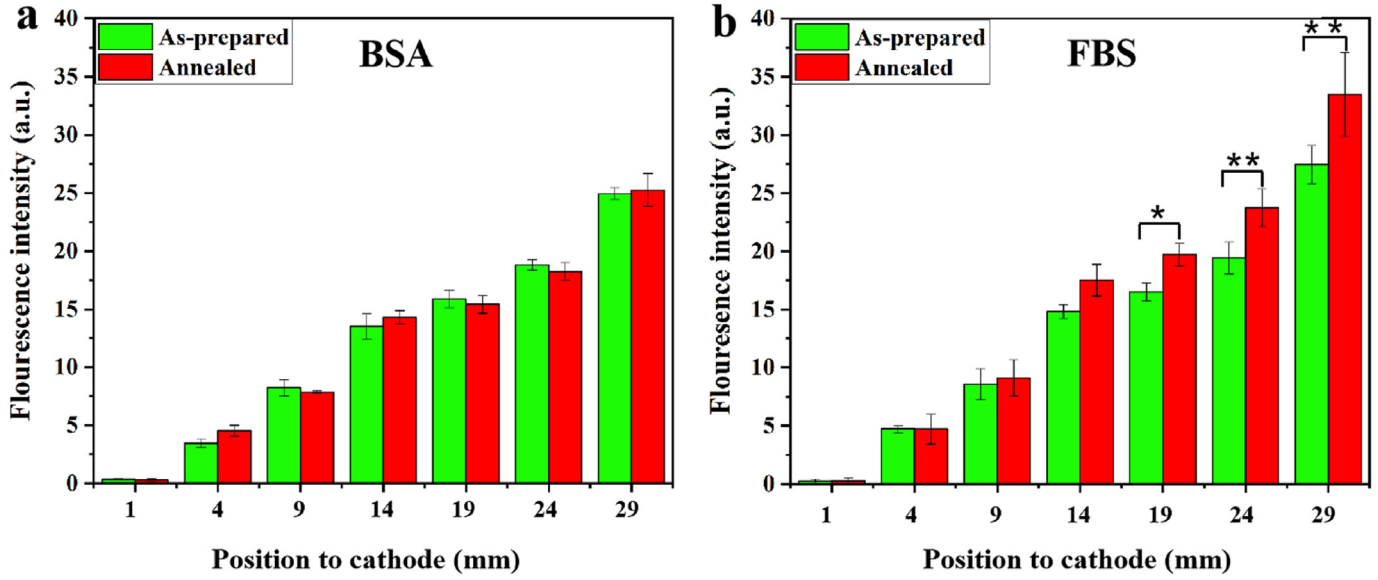

Fig. 3. Fluorescence intensity of adsorbed BSA (a) and serum (b) proteins on different nanotubes of G-TNTs. *p < 0.05 and **p < 0.01 indicate annealed TNTs compared with as-prepared TNTs.

2.4. Cell culture

Rat mesenchymal stem cells (rMSCs) were collected from the femur and tibia of Sprague-Dawley rats (100 g) and expanded in tissue culture polystyrene flasks (TCPS, Thermo scientific) at 37 °C under 5% CO_2 atmosphere. Cell culture media composed of 10% fetal bovine serum (FBS, Gibco) and 1% antibiotics penicillin-streptomycin (HyClone) in alpha-modified minimum essential medium (α-MEM, HyClone). Cells were subcultured at the confluence of 80% and only the first five generations were used for all subsequent cell experiments.

2.5. Cell proliferation

Cell proliferation was evaluated by Calcein-AM (Sigma) staining. Cells were seeded on the gradient samples with a density of 1.0×10^4 cells/cm^2 for 1 day and 3 days. At analysis time, Calcein-AM was cultured with cells for 10 min before fluorescence observation under a fluorescence microscope (TCS SP8, Leica, Germany). Different positions of the gradient TNTs were aligned to the middle of the light source for a thorough examination.

2.6. Cell differentiation

For cell differentiation, the culture medium was replaced after 24 h by induction medium which consisted of high glucose DMEM, 10% FBS, 50 μM ascorbic acid-2-phosphate (Sigma), 100 nM dexamethasone (Sigma), and 10 mM β-glycerophosphate (Sigma).

The early status of cell differentiation was evaluated by alkaline phosphatase kit (Sigma). After 4- and 7-days incubation, samples were washed twice by PBS and fixed by fixative solution (mixing citrate working solution with acetone in a volume ratio of 2:3) for 1 min. Then the mixture of diazonium salt solution (fast blue RR salt) and Naphthol AS-MX phosphate alkaline solution was added to immerse samples at room temperature for 30 min. Subsequently, samples were washed by deionized water before immersing in Mayer's Hematoxylin solution for 10 min, followed by a microscope examination (DM4/6B, Leica).

2.7. Immunofluorescence staining

Cell adhesion was evaluated by immunofluorescence staining of F-actins, vinculins, and nuclei. After cells were cultured for 24 h, gradient samples were rinsed gently by PBS to remove the excess medium. Samples were soaked in 4% paraformaldehyde for 15 min to maintain cell morphology and 0.1% Triton X-100 for 10 min to raise cell membrane permeability to antibodies. Then samples were immersed with 5% BSA for 2 h to avoid nonspecific adsorption. After washing with PBS, samples were incubated with monoclonal anti-vinculin antibody obtained from mouse (1:100, Sigma) at 4 °C for 12 h and anti-mouse IgG-FITC antibody isolated from rabbit (1:100, Sigma) under dark conditions at room temperature for 4 h. Subsequently, 50 μg/ml phalloidin-tetramethyl rhodamine B isothiocyanate (Sigma) was cultured with samples for 30 min at room temperature for actin visualization, followed by nucleus staining with 2 μg/ml 4′,6-diamidino- 2-phenylindole (DAPI, Sigma-Aldrich) for 8 min. After thoroughly rinsed by DI water, samples were examined under confocal microscopy (TCS SP8, Leica, Germany).

2.8. Statistical analysis

Each experiment was performed with at least triplicate. Data were illustrated as mean ± SD and analyzed by One-way analysis of variance (ANOVA) with Turkey post hoc analysis.

3. Results and discussion

3.1. Brief introduction of bipolar electrochemistry

The mechanism of bipolar electrochemistry has been detailed described in the literature [41]. As shown in Scheme 1, two platinum foils are used as feeder electrodes and titanium foil lies in the electrolyte acting as bipolar electrodes (BPE). When powered on, polarization potential appears along the BPE that both reduction and oxidation reactions happen on BPE. Normal anodization takes place at the anodic pole of BPE that TiO_2 nanotubes (TNTs) form. With the decrease of polarization potential, the dimension of TNTs decreases that gradient TNTs (GTNTs) come into shape. Several experimental factors could affect nanotube dimension, including electrolyte type/concentration, applied potential, anodization time, BPE size et al. Different type of electrolyte has been demonstrated to control the shape, dimension of TNTs in single electrochemistry anodization [42]. By scrutinizing literature, we utilize NH_4F/H_2O/Glycerol as the electrolyte and adjust different parameters to obtain GTNTs with a wide diameter range.

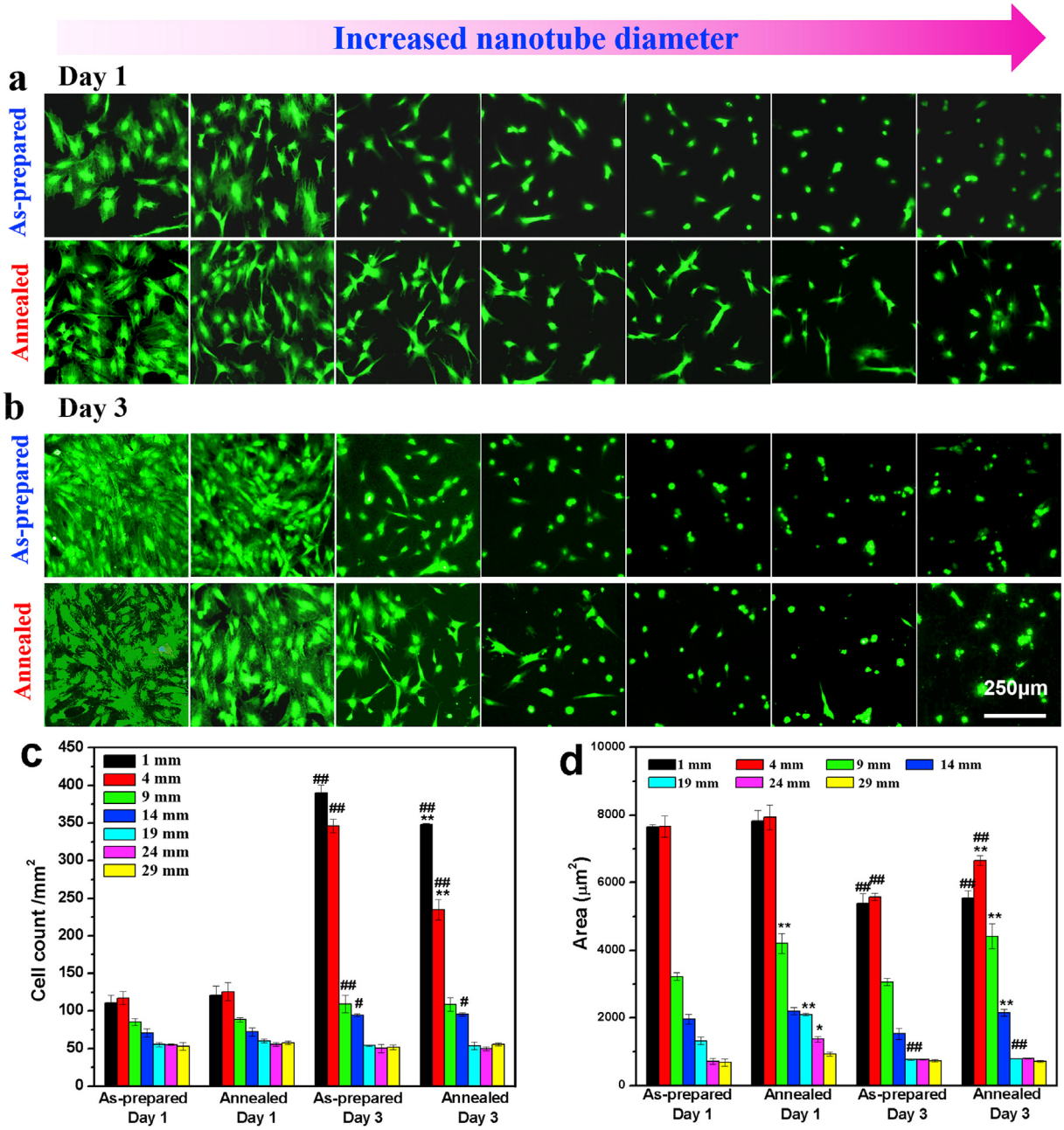

Fig. 4. Fluorescent images of rMSCs cultured on G-TNTs for 1 day (a) and 3 days (b). Cell number (c) and area (d) analyzed by ImageJ. *p < 0.05 and **p < 0.01 indicate annealed TNTs compared with as-prepared TNTs. #p < 0.05 and ##p < 0.01 compared with day 1.

3.2. Characterization of gradient TiO_2 nanotubes

The oxide gradient TNTs covered about 70% of titanium foil (Fig. 1e). As the overpotential on the surface of the bipolar electrode was highest at the anodic edge and decreased towards the middle, nanotubes were distributed on the anodic area and the tube diameter declined through the foil. Fig. 1a shows highly ordered SEM micrographs of the as-prepared and annealed gradient TiO_2 nanotube arrays. The outer diameter of gradient nanotubes ranged from ~20 nm to ~350 nm (Fig. 1b), the wall thickness ranged from ~5 nm to ~35 nm (Fig. 1c), and the nanotube length ranged from ~0.2 μm to ~2.8 μm (Fig. 1d and Fig. S2). Adjacent to the smallest nanotubes, the surface was relatively flat. But as it has gone through anodization under low potential, a thin layer of TiO_2 could be expected and it was utilized as a control for the following experiments. Nanotubular structures were retained after high-temperature annealing. Nanotube wall thickness rises slightly without significant difference (Fig. 1c).

X-ray diffraction is a standard technique for structural analysis. Herein, we utilized XRD to thoroughly characterize the crystallize phases of the TNTs by aligning different positions of the gradient with the X-ray beam. However, as all TNTs with different dimensions were integrated within one gradient sample, one has to bear in mind that the focal spot size of the X-ray spectrometer is about 5 mm × 12 mm in this study and the results could only reflect the change across the sample, not the results for the specific positions. The XRD patterns in Fig. 2a shows that, for the as-prepared gradient TNTs, there were no significant phase components such as brookite, anatase, or rutile. The peak located at 2θ value of 25.3° in Fig. 2b could be indexed to the (101) reflection of the anatase phase (JCPDS No. 21–1272). Only anatase phase was detected on the annealed gradient TNTs and the intensity was relatively low on the small nanotube region and vanished on the flat TiO_2 area.

Different from XRD, the spot size of the Raman laser beam can be as

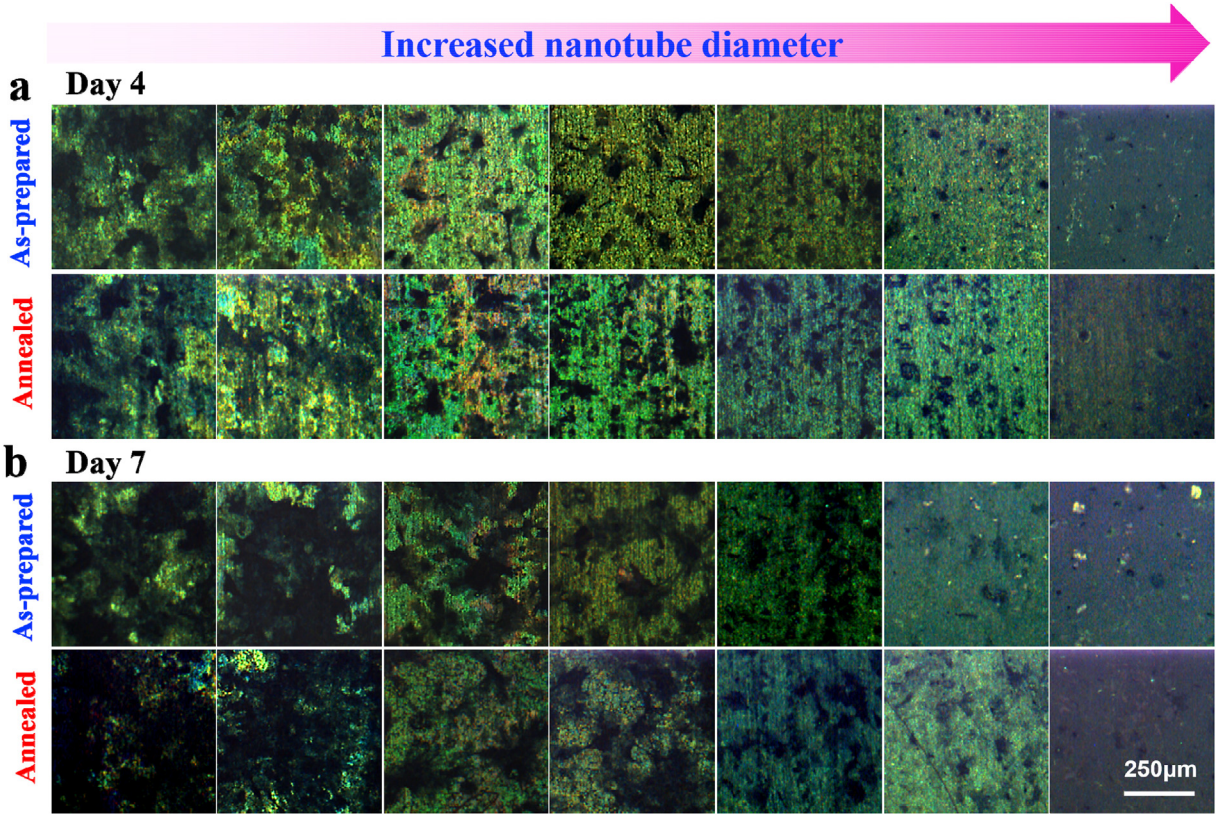

Fig. 5. Optical images of alkaline phosphatase production on gradient TiO_2 nanotubes after cell culture for 4 days (a) and 7 days (b).

small as ~500 nm that it could detect weak signals. Thus, Raman spectroscopy was also employed to assess the crystalline information. Different positions on the sample were examined by aligning different locations to the middle of the Raman active region. The Raman spectra in Fig. 2c and d shows four wide vibration bands at the range of 100–900 cm^{-1}. There was no distinct vibration peak for most areas of the as-prepared gradient nanotubes (Fig. 2c). Most annealed gradient TNTs presented characteristic Raman bands near 143 cm^{-1} (E_g), 197 cm^{-1} (E_g), 395 cm^{-1} (B_{1g}), 517 cm^{-1} (A_{1g}), and 640 cm^{-1} (E_g) [43] which is congruous with XRD observations. An enlargement of the Raman spectra of the flat TiO_2 and smallest nanotube areas (Fig. 2d, enlarged image) shows weak Raman bands located at 447 cm^{-1} (E_g), and 612 cm^{-1} (A_{1g}), which could be assigned to rutile phase [43]. Interestingly, however, the as-prepared TNTs with the largest diameter (~350 nm) displayed a strong peak at 150 cm^{-1} and three wide peaks at about 404, 502, and 623 cm^{-1} (Fig. 2c). These Raman modes seem similar to those of anatase nanotube, however, the main vibration E_g peak shifted toward 150 cm^{-1} and the B_{1g} peak shifted toward 404 cm^{-1}. Those two peaks indicate the presence of the brookite phase [44]. However, the brookite phase usually has many Raman bands [45] and the other two peak positions are not a good match. Given those nanotubes were as-prepared without further annealing and three peaks were relatively wide, we can reasonably speculate that the crystals are not pure. The appearance of crystalline phases in the as-prepared samples may be related to the high energy and driving force generated by high voltage, causing a certain rearrangement of Ti and O atoms [46,47].

The discrepancy between Raman and XRD data could be ascribed to the difference between those two techniques, with XRD usually requires a certain sample size and good crystals. As mentioned above, the focal spot size of the X-ray spectrometer is about 5 mm × 12 mm that the anatase peak emerged in the XRD spectra of the smallest nanotube area might come from the nearby nanotubes. And as the TiO_2 film in the region of the flat TiO_2 and smallest nanotubes is thin (−200 nm) and the amount is relatively small, it is difficult for X-ray spectrometer to detect the rutile phase. In contrast, the spot size of the Raman laser beam used in this study was about 500–600 nm that it could detect weak signals. Similarly, Raman spectroscopy detected a small amount of impure brookite phase on the as-prepared TNTs whereas there was no detectable XRD peak.

Surface wettability of the as-prepared and annealed gradient TNTs was investigated by the water contact angle (Fig. S3). There was no distinct difference between annealed and as-prepared samples. The flat area had a water contact angle of about 65°, suggesting the flat TiO_2 surface is hydrophilic. All the nanotubes exhibited excellent wettability with water contact angles below 10°, and there was no significant difference among TNTs with different diameters.

3.3. Protein adsorption

As one of the first occurrences at the course of cell-material interaction, protein adsorption can affect cell behaviors and osteogenesis. Herein, the adsorptive ability of proteins on different sized TiO_2 nanotubes was qualitatively analyzed by the fluorescence of adsorbed proteins. As shown in Fig. 3a, for both as-prepared and annealed gradient TNTs, BSA protein adsorption was lowest on the flat TiO_2 surface and increased constantly with the enlargement of nanotube diameter. It can be ascribed to the increased nanotube length of larger nanotube which amplifies the exposed surface area. But there was no noteworthy fluorescence difference of labeled BSA between the as-prepared and annealed TNTs with the same dimension. A similar adsorption pattern was observed for serum proteins except relative higher adsorption could be found on large diameter regions on annealed GTNTs (Fig. 3b). This could be owing to the synergistic effects of surface properties and competitive protein adsorption in serum [35]. Different properties had different effects on protein adsorption that combined effects of varied properties could be found on protein adsorption, including crystalline phase, surface chemistry, and wettability. Moreover, serum proteins

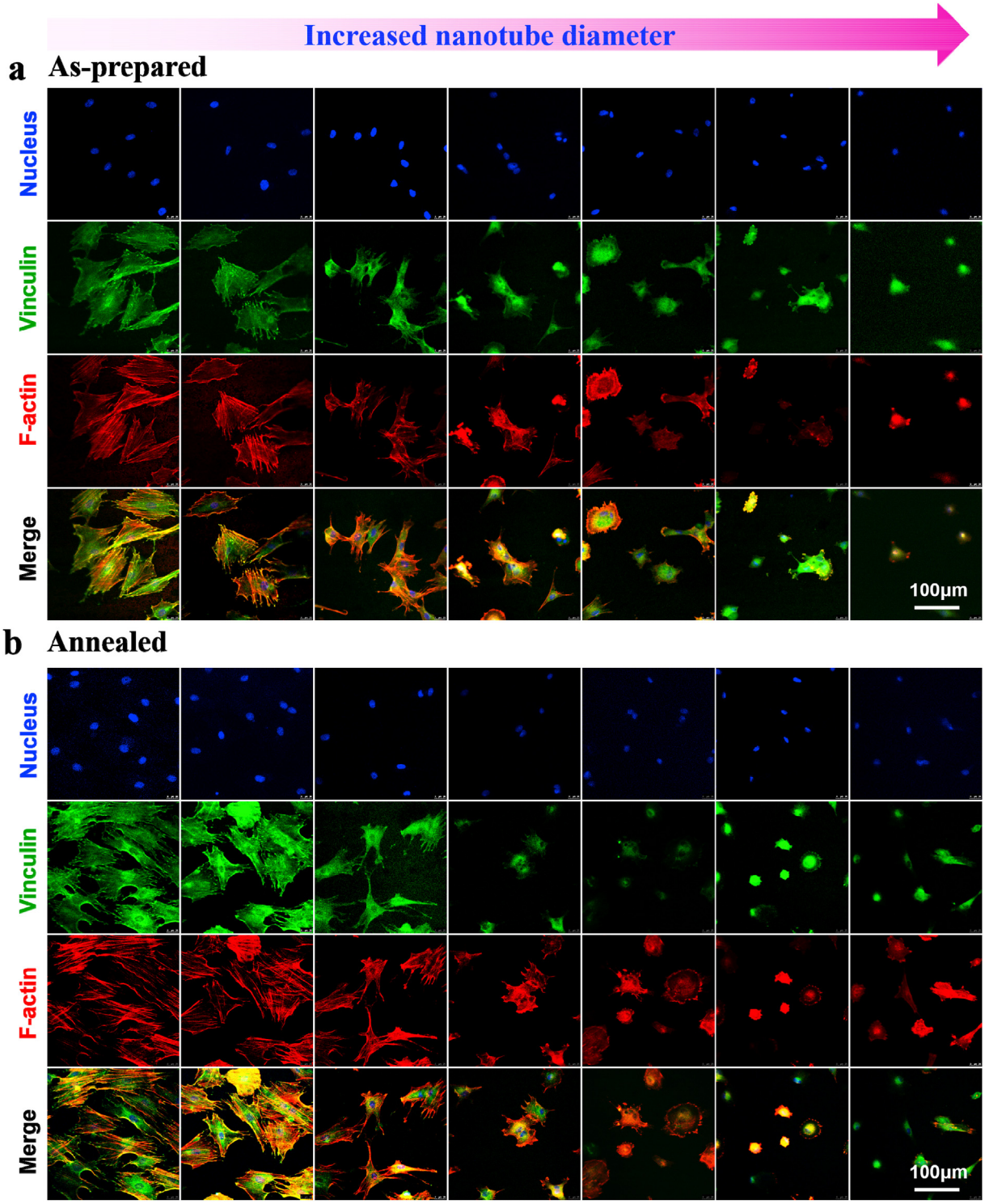

Fig. 6. Fluorescence images of rMSCs stained with nuclei, vinculins, and F-actins after one-day culture: (a) as-prepared and (b) annealed GTNTs.

consist of thousands of proteins varied in size, charge, concentration. The variety in serum proteins and competitive adsorption also adds to the synergistic effects of crystalized TNTs on serum protein adsorption.

3.4. Cell proliferation

To assess cell proliferation on gradient TiO_2 nanotube arrays, cells were stained with calcein-AM after cultured for 1 day and 3 days. As depicted in Fig. 4a, on the as-prepared GTNTs, more cells attached to the flat TiO_2 and small nanotube regions with apparent lamellipodium on day one. The number of adherent cells gradually declined with the increment of nanotube diameter. Besides, cells shrank from a well-spread shape to fewer extensions/filopodia or even round shape. Cells response to annealed GTNTs was similar except cell spread better on the annealed nanotubes with diameters larger than 70 nm (Fig. 4a and d, day 1, compare as-prepared sample to annealed sample).

After three days of proliferation, cell behaviors on as-prepared and annealed samples were similar. Cell density on the flat TiO_2 and small nanotube regions (< 70 nm) increased notably (Fig. 4b and c). But cell size diminished prominently (Fig. 4d) owing to the overcrowding. Cell

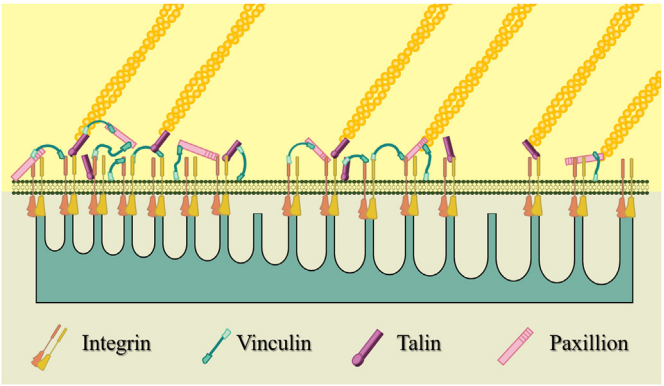

Fig. 7. Schematic diagram of cell adhesion on GTNTs with different dimensions.

numbers only increased slightly on nanotubes with a diameter range of 70–120 nm without significant change in cell size, even though it was sufficiently spacious to hold more cells. Cells were mostly spherical with no conspicuous cell growth for nanotubes with a diameter larger than 180 nm. This validates our previous research that small-sized nanotubes are more conducive to cell proliferation [28].

3.5. Cell differentiation

Alkaline phosphatase (ALP) is an early marker of osteogenesis that the early differentiation level of rMSCs could be detected by the production of ALP. Fig. 5 showed a similar trend of ALP expression on both as-prepared and annealed GTNTs. After 4 days of osteogenic induction, the expression of ALP was highest on flat TiO_2 and smallest TNTs regions. But the activity of ALP decreased with the increase of nanotube size. Compared to non-annealed samples, a slight increase of ALP expression could be observed in the diameter region of 120–245 nm on annealed GTNTs. On day 7, a remarkable increase in ALP product was found on TNTs with diameters smaller than 180 nm for both as-prepared and annealed GTNTs. ALP aggregation emerged on the nanotubes with a diameter smaller than 120 nm, indicating their high activity for osteogenic differentiation.

The nucleus is the control center of the cell, storing genetic materials and manipulating metabolic activities. Vinculin connects integrin and cytoskeleton actin, and plays an extremely important role in microfilament-mediated cell movement, controlling cell adhesion, spreading, movement, proliferation, and signal transmission. The cytoskeleton, mainly composed of skeletal proteins and actin, is a filamentous network structure. Besides, to support cell shape, resist deformation, and provide signaling pathways, the cytoskeleton also participates in cell migration and differentiation [48,49]. To further understand cell behavior, cell nucleus, vinculin, and F-actin were stained after one-day culture on gradients. As shown in Fig. 6a, compared the as-prepared TNTs to the annealed TNTs with the same dimension, cell behaviors were similar and there was no significant difference in vinculin distribution or actin cytoskeleton. It explains why the effects of crystalline phases on cell behaviors are not significant through the entire gradient, consistent with our previous study [35]. A reasonable explanation is that the synergistic effects of different surface properties and competitive protein adsorption diminish the difference between as-prepared TNTs and annealed TNTs.

On the flat TiO_2 and small diameter nanotubes, the nucleus was plump with natural shape. The actin cytoskeleton was highly organized and densely distributed. Labeled green vinculin was well distributed in cells and aggregated at the periphery of lamellipodia and filopodium. The size of the aggregated vinculin is about 3 μm. As the diameter of the tube increases, cell spreading was reduced that the size of the nucleus diminished, together with blurred actin cytoskeleton and vanished vinculin clusters.

As one of the membrane-cytoskeletal proteins in focal adhesion, vinculin aggregations indicate the formation of focal adhesion. Apparently, small size nanotubes can provide more anchor sites at the top of nanotubes for protein adsorption which facilitate the following process of extracellular matrix formation, integrin binding, vinculin/talin/paxillin interconnecting and focal adhesion assembly (Fig. 7). On the other hand, large-size-nanotubes have abundant surface area and can adsorb more proteins (Fig. 3) because the tubes are longer. However, the wide-open tubes disconnect ECM and further prejudice the formation of focal adhesion. As focal adhesion is crucial to cell attachment, spreading, proliferation and differentiation, small diameter nanotubes have superiority for cell adhesion and growth.

4. Conclusions

In summary, we utilized bipolar electrochemistry to achieve GTNTs with a wide diameter range of 20–350 nm. GTNTs were further applied to investigate the size and crystalline phase effects of TNTs on protein adsorption and cellular behaviors. Results show that larger diameter TiO_2 nanotubes exhibit a higher capacity for protein adsorption, while small diameter nanotubes are more conducive to cell adhesion, proliferation, and differentiation. Annealed large diameter nanotubes (diameter $>$ 180 nm) adsorb more serum proteins than as-prepared ones whereas no prominent difference in BSA adsorption. Cell proliferation was higher on the as-prepared flat TiO_2 and 20 nm diameter regions than annealed ones whereas no observable difference on other nanotubes. Cell differentiation varied with nanotube dimension whereas no discernible ALP activity between as-prepared and annealed TNTs with the same dimension. This study extends our previous research about protein adsorption and cell behaviors on GTNTs, enhancing our understanding of nanotube dimension and annealing effect on protein adsorption and cell behaviors at a larger extend.

CRediT authorship contribution statement

Yanran Li: Investigation, Visualization, Writing - original draft. **Si Wang:** Investigation. **Yuanjun Dong:** Investigation. **Ping Mu:** Methodology, Investigation. **Yun Yang:** Writing - review & editing. **Xiangyang Liu:** Resources. **Changjian Lin:** Resources. **Qiaoling Huang:** Conceptualization, Supervision, Visualization, Writing - review & editing.

Declaration of competing interest

The authors declare no conflict of interest.

Acknowledgments

The authors appreciate funding assistants from the State Key Project of Research and Development (2016YFC1100300), National Natural Science Foundation of China (11904301, 21773199), Natural Science Foundation of Guangdong Province, China (2016A030310370) and 111 Project (B16029). The authors would like to thank Hao Wang, Rui Yu and Likun Yang for their technical supports.

Appendix A. Supplementary data

Supplementary data to this article can be found online at https://doi.org/10.1016/j.bioactmat.2020.07.005.

References

[1] X. Ge, C. Ren, Y. Ding, G. Chen, X. Lu, K. Wang, et al., Micro/nano-structured TiO_2 surface with dual-functional antibacterial effects for biomedical applications, Bioact. Mater. 4 (2019) 346–357.

[2] L. Huang, K. Su, Y.-F. Zheng, K.W.-K. Yeung, X.-M. Liu, Construction of TiO_2/silane nanofilm on AZ31 magnesium alloy for controlled degradability and enhanced biocompatibility, Rare Met. 38 (6) (2019) 588–600.

[3] X. Zhang, Y. Huang, B. Wang, X. Chang, H. Yang, J. Lan, et al., A functionalized Sm/Sr doped TiO_2 nanotube array on titanium implant enables exceptional bone-implant integration and also self-antibacterial activity, Ceram. Int. 46 (10, Part A) (2020) 14796–14807.

[4] Y. Wang, D. Zhang, C. Wen, Y. Li, Processing and characterization of $SrTiO_3$–TiO_2 nanoparticle–nanotube heterostructures on titanium for biomedical applications, ACS Appl. Mater. Interfaces 7 (29) (2015) 16018–16026.

[5] J.M. Zhang, Y.H. Sun, Y. Zhao, Y.L. Liu, X.H. Yao, B. Tang, et al., Antibacterial ability and cytocompatibility of Cu-incorporated Ni–Ti–O nanopores on NiTi alloy, Rare Met. 38 (6) (2019) 552–560.

[6] S. Hejazi, S. Mohajernia, B. Osuagwu, G. Zoppellaro, P. Andryskova, O. Tomanec, et al., On the controlled loading of single platinum atoms as a Co-catalyst on TiO_2 anatase for optimized photocatalytic H_2 generation, Adv. Mater. (2020) 1908505.

[7] Z.Y. Xiu, M.J. Guo, T.Y. Zhao, K. Pan, Z.P. Xing, Z.Z. Li, et al., Recent advances in Ti^{3+} self-doped nanostructured TiO_2 visible light photocatalysts for environmental and energy applications, Chem. Eng. J. 382 (2020) 123011.

[8] H.J. Li, Y. Zhou, W.G. Tu, J.H. Ye, Z.G. Zou, State-of-the-art progress in diverse heterostructured photocatalysts toward promoting photocatalytic performance, Adv. Funct. Mater. 25 (7) (2015) 998–1013.

[9] V. Galstyan, A. Ponzoni, I. Kholmanov, M.M. Natile, E. Comini, G. Sberveglieri, Highly sensitive and selective detection of dimethylamine through Nb-doping of TiO_2 nanotubes for potential use in seafood quality control, Sensor. Actuator. B Chem. 303 (2020) 127217.

[10] A.V. Lashkov, F.S. Fedorov, M.Y. Vasilkov, A.V. Kochetkov, I.V. Belyaev, I.A. Plugin, et al., The Ti wire functionalized with inherent TiO_2 nanotubes by anodization as one-electrode gas sensor: a proof-of-concept study, Sensor. Actuator. B Chem. 306 (2020) 127615.

[11] L.K. Yang, X. Wang, X.M. Mai, T. Wang, C. Wang, X. Li, et al., Constructing efficient mixed-ion perovskite solar cells based on TiO_2 nanorod array, J. Colloid Interface Sci. 534 (2019) 459–468.

[12] W.P. Hu, W.R. Zhou, X.Y. Lei, P.C. Zhou, M.M. Zhang, T. Chen, et al., Low-temperature in situ amino functionalization of TiO_2 nanoparticles sharpens electron management achieving over 21% efficient planar perovskite solar cells, Adv. Mater. 31 (8) (2019) 1806095.

[13] Y. Lai, Y. Cheng, H. Yang, Y. Yang, J. Huang, Z. Chen, et al., Progress in TiO_2 nanotube coatings for biomedical applications: a review, J. Mater. Chem. B 6 (2018) 1862.

[14] M.F. Kunrath, R. Hubler, R.S.A. Shinkai, E.R. Teixeira, Application of TiO_2 nanotubes as a drug delivery system for biomedical implants: a critical overview, ChemistrySelect 3 (40) (2018) 11180–11189.

[15] M.G. Necula, A. Mazare, R.N. Ion, S. Ozkan, J. Park, P. Schmuki, et al., Lateral Spacing of TiO_2 nanotubes modulates osteoblast behavior, Materials 12 (18) (2019) 2956.

[16] M.F. Dias-Netipanyj, K. Cowden, L. Sopchenski, S.C. Cogo, S. Elifio-Esposito, K.C. Popat, et al., Effect of crystalline phases of titania nanotube arrays on adipose derived stem cell adhesion and proliferation, Mater. Sci. Eng. C 103 (2019) 109850.109850.109851-109850.109858.

[17] J.R. Leon-Ramos, J.M. Diosdado-Cano, C. Lopez-Santos, A. Barranco, D. Torres-Lagares, M.A. Serrera-Figallo, Influence of titanium oxide pillar array nanometric structures and ultraviolet irradiation on the properties of the surface of dental implants-a pilot study, Nanomaterials 9 (10) (2019) 1458.

[18] Z.H. Gong, Y.D. Hu, F. Gao, L. Quan, T. Liu, T. Gong, et al., Effects of diameters and crystals of titanium dioxide nanotube arrays on blood compatibility and endothelial cell behaviors, Colloids Surf., B 184 (2019) 1105212.

[19] Y. Yang, L.H. Liu, H. Luo, D. Zhang, S.R. Lei, K.C. Zhou, Dual-purpose magnesium-incorporated titanium nanotubes for combating bacterial infection and ameliorating osteolysis to realize better osseointegration, ACS Biomater. Sci. Eng. 5 (10) (2019) 5368–5383.

[20] U.F. Gunputh, H.R. Le, K. Lawton, A. Besinis, C. Tredwin, R.D. Handy, Antibacterial properties of silver nanoparticles grown in situ and anchored to titanium dioxide nanotubes on titanium implant against Staphylococcus aureus, Nanotoxicology 14 (1) (2020) 97–110.

[21] M.H. Kafshgari, W.H. Goldmann, Insights into theranostic properties of titanium dioxide for nanomedicine, Nano-Micro Lett. 12 (1) (2020) 35.

[22] Y. Liu, C.L. Xie, F.F. Zhang, X.F. Xiao, pH-responsive TiO_2 nanotube drug delivery system based on iron coordination, J. Nanomater. 2019 (2019) 6395760.

[23] J. Barthes, S. Ciftci, F. Ponzio, H. Knopf-Marques, L. Pelyhe, A. Gudima, et al., Review: the potential impact of surface crystalline states of titanium for biomedical applications, Crit. Rev. Biotechnol. 38 (3) (2018) 423–437.

[24] N.K. Awad, S.L. Edwards, Y.S. Morsi, A review of TiO_2 NTs on Ti metal: electrochemical synthesis, functionalization and potential use as bone implants, Mater. Sci. Eng. C 76 (2017) 1401–1412.

[25] J. Park, S. Bauer, P. Schmuki, K. von der Mark, Narrow window in nanoscale dependent activation of endothelial cell growth and differentiation on TiO_2 nanotube surfaces, Nano Lett. 9 (9) (2009) 3157–3164.

[26] J. Park, S. Bauer, K.A. Schlegel, F.W. Neukam, K. von der Mark, P. Schmuki, TiO_2 nanotube surfaces: 15 nm - an optimal length scale of surface topography for cell adhesion and differentiation, Small 5 (6) (2009) 666–671.

[27] K. von der Mark, S. Bauer, J. Park, P. Schmuki, Another look at "Stem cell fate dictated solely by altered nanotube dimension, Proc. Natl. Acad. Sci. U.S.A. 106 (24) (2009) E60.

[28] P. Mu, Y. Li, Y. Zhang, Y. Yang, R. Hu, X. Zhao, et al., High-throughput screening of rat mesenchymal stem cell behavior on gradient TiO_2 nanotubes, ACS Biomater. Sci. Eng. 4 (8) (2018) 2804–2814.

[29] S. Oh, K.S. Brammer, Y.S.J. Li, D.Y. Teng, A.J. Engler, S. Chien, et al., Reply to von der Mark et al.: looking further into the effects of nanotube dimension on stem cell fate, Proc. Natl. Acad. Sci. U.S.A. 106 (24) (2009) E61.

[30] S. Oh, K.S. Brammer, Y.S.J. Li, D. Teng, A.J. Engler, S. Chien, et al., Stem cell fate dictated solely by altered nanotube dimension, Proc. Natl. Acad. Sci. U.S.A. 106 (7) (2009) 2130–2135.

[31] K.S. Brammer, S. Oh, C.J. Cobb, L.M. Bjursten, Hvd Heyde, S. Jin, Improved bone-forming functionality on diameter-controlled TiO_2 nanotube surface, Acta Biomater. 5 (8) (2009) 3215–3223.

[32] W.Q. Yu, Y.L. Zhang, X.Q. Jiang, F.Q. Zhang, In vitro behavior of MC3T3-E1 pre-osteoblast with different annealing temperature titania nanotubes, Oral Dis. 16 (7) (2010) 624–630.

[33] Y. Bai, S. Park, H.H. Park, M.H. Lee, T.S. Bae, W. Duncan, et al., The effect of annealing temperatures on surface properties, hydroxyapatite growth and cell behaviors of TiO_2 nanotubes, Surf. Interface Anal. 43 (6) (2011) 998–1005.

[34] R. Zhang, H. Wu, J. Ni, C. Zhao, Y. Chen, C. Zheng, et al., Guided proliferation and bone-forming functionality on highly ordered large diameter TiO_2 nanotube arrays, Mater. Sci. Eng. C 53 (2015) 272–279.

[35] Y. Li, Y. Dong, Y. Zhang, Y. Yang, R. Hu, P. Mu, et al., Synergistic effect of crystalline phase on protein adsorption and cell behaviors on TiO_2 nanotubes, Appl. Nanosci. 106 (2019) 1–13.

[36] McAlear JH, Wehrung JM. Microdevice substrate and method for making micropattern devices. Google Patents. (1978).

[37] J. Seo, J.Y. Shin, J. Leijten, O. Jeon, G. Camci-Unal, A.D. Dikina, et al., High-throughput approaches for screening and analysis of cell behaviors, Biomaterials 153 (2018) 85–101.

[38] P. Machillot, C. Quintal, F. Dalonneau, L. Hermant, P. Monnot, K. Matthews, et al., Automated buildup of biomimetic films in cell culture microplates for high-throughput screening of cellular behaviors, Adv. Mater. 30 (27) (2018) 1801097.

[39] A. Pittrof, J. Park, S. Bauer, P. Schmuki, ECM spreading behaviour on micro-patterned TiO_2 nanotube surfaces, Acta Biomater. 8 (7) (2012) 2639–2647.

[40] Y. Chen, J. Ni, H. Wu, R. Zhang, C. Zhao, W. Chen, et al., Study of cell behaviors on anodized TiO_2 nanotube arrays with coexisting multi-size diameters, Nano-Micro Lett. 8 (1) (2015) 61–69.

[41] S.O. Krabbenborg, J. Huskens, Electrochemically generated gradients, Angew. Chem. Int. Ed. 53 (35) (2014) 9152–9167.

[42] K. Lee, A. Mazare, P. Schmuki, One-dimensional titanium dioxide nanomaterials: nanotubes, Chem. Rev. 114 (19) (2014) 9385–9454.

[43] P. Kar, Y. Zhang, S. Farsinezhad, A. Mohammadpour, B.D. Wiltshire, H. Sharma, et al., Rutile phase n- and p-type anodic titania nanotube arrays with square-shaped pore morphologies, Chem. Commun. 51 (37) (2015) 7816–7819.

[44] L. Gang, G.Y. Hua, C. Sun, L. Cheng, H.M. Cheng, Titania polymorphs derived from crystalline titanium diboride, CrystEngComm 11 (12) (2009) 2677–2682.

[45] J. Xu, K. Li, S. Wu, W. Shi, T. Peng, Preparation of brookite titania quasi nanocubes and their application in dye-sensitized solar cells, J. Mater. Chem. 3 (14) (2015) 7453–7462.

[46] J.M. Macak, H. Hildebrand, U. Marten-Jahns, P. Schmuki, Mechanistic aspects and growth of large diameter self-organized TiO_2 nanotubes, J. Electroanal. Chem. 621 (2) (2008) 254–266.

[47] M.V. Diamanti, M.P. Pedeferri, Effect of anodic oxidation parameters on the titanium oxides formation, Corrosion Sci. 49 (2) (2007) 939–948.

[48] D.A. Fletcher, R.D. Mullins, Cell mechanics and the cytoskeleton, Nature 463 (7280) (2010) 485–492.

[49] H. Herrmann, H. Bar, L. Kreplak, S.V. Strelkov, U. Aebi, Intermediate filaments: from cell architecture to nanomechanics, Nat. Rev. Mol. Cell Biol. 8 (7) (2007) 562–573.